Research Article | Vol. 30, No. 4 / 14 Feb 2022 / Optics Express 4692

Maximizing energy utilization in DMD-based projection lithography

MING-JIE DENG,[1] YUAN-YUAN ZHAO,[1,2] ZI-XIN LIANG,[1] JING-TAO CHEN,[1] YANG ZHANG,[1] AND XUAN-MING DUAN[1,3]

[1]Guangdong Provincial Key Laboratory of Optical Fiber Sensing and Communications, Institute of Photonics Technology, Jinan University, Guangzhou 511443, China
[2]yyzhao@jnu.edu.cn
[3]xmduan@jnu.edu.cn

Abstract: In digital micromirror device (DMD)-based projection photolithography, the throughput largely depends on the effectiveness of the laser energy utilization, which is directly correlated to the diffraction efficiency of DMD. Here, to optimize the DMD diffraction efficiency and thus the laser energy utilization, we calculate the diffraction efficiencies $E_{diffraction}$ of DMD with various pitch sizes at wavelengths ranging from 200 nm to 800 nm, using the two-dimensional blazed grating diffraction theory. Specifically, the light incident angle is optimized for 343 nm laser and 7.56 µm pitch-size DMD, and the maximum single-order diffraction efficiency $E_{diffraction}$ is increased from 40% to 96%. Experimentally, we use the effective energy utilization $\eta_{eff} = E_{diffraction,(m,n)}/\Sigma[E_{diffraction,(m,n)}]$ at the entrance pupil plane of the objective to verify the effectiveness of the optimized illumination angle in a lithography illumination system with parallel beams of two wavelengths (343 nm and 515 nm). The η_{eff} of a "blaze" order at a 34° angle of incidence can be optimized up to 88%. The experimental results are consistent with the tendency of the calculated results, indicating that this optimization model can be used to improve the energy utilization of projection lithography with the arbitrarily designable wavelengths and the DMD's pitch size.

© 2022 Optica Publishing Group under the terms of the Optica Open Access Publishing Agreement

1. Introduction

Digital micromirror devices (DMD)-based projection lithography (DMD-PL), as a promising alternative technique for traditional photolithography, has received a lot of attention in the last decades [1–3]. Benefiting from its higher manufacturing efficiency and lower cost [4,5], DMD-PL meets the current urgent needs for rapid [6–8] and economical fabrication of micro-/nanodevices [9–11]. The resolution of the conventional DMD-PL has been constrained to the sub-micrometer region for a long time due to the diffraction limit. In recent years, the resolution of DMD-PL has been significantly improved and achieved nanometer scale by the two-photon absorption effect of photoresists [12,13]. The resolution is expected to be further improved by continuously reducing the pixel size of the DMD (see Texas Instruments Products, TI), increasing the magnification of the projection objective, and shortening the wavelength of the ultrafast laser. In DMD-PL systems, the laser beam collimated with a flat-topped energy distribution is incident on the DMD at a fixed azimuth and incident angle [14], and the output beam comprises a lot of diffraction orders with the discrete angles due to the grid effect [15,16]. The optical objective lens receives one or several diffraction orders as object information for exposure. The evolution of the pixel (micromirror) size of the DMD and the wavelength of the laser will affect the imaging quality and the energy utilization of the light source [17]. As discussed in TI's published white paper [18–20], overall energy utilization η_{DMD} can be estimated using Eq. (1).

$$\eta_{DMD} = (T_{window})^2 \times E_{fill.factor} \times E_{diffraction} \times R_{mirror} = C \times E_{diffraction} \tag{1}$$

where C stands for an intrinsic parameter of DMD determined by its physical structures.

#448231 https://doi.org/10.1364/OE.448231
Journal © 2022 Received 11 Nov 2021; revised 16 Jan 2022; accepted 16 Jan 2022; published 31 Jan 2022

- T_{window} is single-pass window transmission. This term is accounted for twice because light travels through the window twice. A single pass average transmittance T_{window} is $\geq 99\%$.
- $E_{\text{fill.factor}}$ is the fractional mirror coverage (on-state mirrors) as viewed from the illumination direction. Typical on-state fill factor $E_{\text{fill.factor}}$ is $\geq 92\%$.
- R_{mirror} is the mirror reflectivity including mirror scatter. The mirrors are nominally 89% reflective in the visible range.
- $E_{\text{diffraction}}$ is the diffraction efficiency of DMD which is affected by the pixel size, laser wavelength and incident angle.

The diffraction efficiency $E_{\text{diffraction}}$ of DMD is the main determinant of the overall energy utilization η_{DMD} [18]. When a DMD is illuminated with coherent, collimated, narrow-band light, the reflected diffraction light is a two-dimensional (2D) pattern of spots called "diffraction orders" [21,22]. A "blaze" condition exists when one diffraction order contains most of the energy in the overall diffraction pattern. An "anti-blaze" condition exists when the four brightest orders contain equal amount of energy in the diffraction pattern. A "blaze" or an "anti-blaze" condition may exist depending on the pixel pitch, micromirror tilt angle, illumination wavelength, and the incident angle of the illumination light [20]. The pixel sizes of available commercial DMD (TI Products) are 13.68, 10.8, 7.56 and 5.4 μm [23], respectively. Although using DMD with smaller pixel size generally improves the resolution of DMD-PL [24,25], the smaller micromirror will aggravate the diffraction effect and affect the energy utilization efficiency and the spatial distribution of diffraction order [26–28]. In DMD-PL, a variety of wavelengths ranging from ultraviolet to near infrared have been used to suit the needs of different technologies and applications [29–32]. In addition, due to the limitation of the entrance pupil of the projection objective, generally only a single diffraction order can enter a high de-magnification lithography system [18,19]. Improving the diffraction efficiency of a single order and improving the energy utilization are the key problems to be solved in lithography. Therefore, for the complex and changeable diffraction characteristics of DMD [33–36], it is necessary to establish a complete parameter model for analyzing specific conditions, optimizing illumination angles and improving the energy utilization in lithography.

In this work, we systematically examine the impact of multiple parameters such as the size of the pixels, operating wavelength, incident angle, projection objective's pupil aperture, and working distance, on the energy utilization rate of the lithography system. A broadband (200 nm - 800 nm) two-angle (azimuth and incident angles) variable DMD diffraction model is established and used to analyze the energy envelope and diffraction order distribution in variable cases, and optimize the incident angle for maximum energy utilization in DMD-PL. Furthermore, the experiments employed lasers with the wavelengths of 343 nm and 515 nm are performed for validating the DMD diffraction model. The experimental results agree well with the simulation results, which confirms the accuracy of the model. The maximum diffraction efficiency for 343 nm laser and 7.56 μm DMD is 96% at an optimized light incident angle of 34° in theory. The diffraction model developed here can be used as a powerful tool for maximizing laser energy utilization in various DMD-PLs.

2. DMD diffraction model

2.1. DMD diffraction order and phase distribution

Figure 1(a) shows a typical DMD-based projection lithography system. In general, a DMD can be considered as a modulated 2D blazed grating. Each diffraction order can be used alone as to carry object information, and the objective lens collects one or several orders to complete the exposure on the photoresist. Figure 1(b) shows the operation mode (non-TRP) [37] of DMD with pixels

sizes of 13.68 μm, 10.8 μm, and 7.56 μm. The corresponding DMD numbers are (DLP7000 & 13.68 μm), (DLP6500, DLP650LE & 10.8 μm), (DLP303X, DLP553X, DLP4501, DLP9000 & 7.56 μm). The single rectangular micromirror area is defined as $d_{DMD} \times d_{DMD}$. The light source is input from the diagonal, and the energy envelope outgoing direction is perpendicular to the backplane when DMD's state is open. The beam deflection angle is ±12° corresponding to two states (on and off) of switching. The grating constant d and blaze angle γ of the equivalent blazed grating are $d_{DMD}/1.414$ and 12°, respectively. The operation mode (TRP) [37] of 5.4 μm pixel size DMD is shown in Fig. 1(c). The corresponding DMD numbers are DLP3010 & 5.4 μm. The micromirrors first rotate 12° around the diagonal 1 and then 12° around the diagonal 2, resulting in a compound deflection angle of ±17° around the central axis. The incident light becomes side incident, and the energy envelope exits perpendicular to the backplane. Accordingly, the grating constant d and blaze angle γ of the equivalent blazed grating become d_{DMD} and 17°, respectively. In addition, each mirror has a rectangular hole of about 2 microns in the center, and the interval between two adjacent mirrors is less than 1 μm [38]. This special structure leads to a decrease in energy utilization. We can use the filling factor $E_{\text{fill.factor}}$ to characterize the energy loss (see Eq. (1)) [20]. Consequently, when the parallel beam is incident on the DMD at an angle of 2γ to the normal direction and the state of the DMD micromirrors is controlled by the pre-loaded binary patterns with a laser light, the outgoing diffraction patterns can be used as a digital mask for projection lithography.

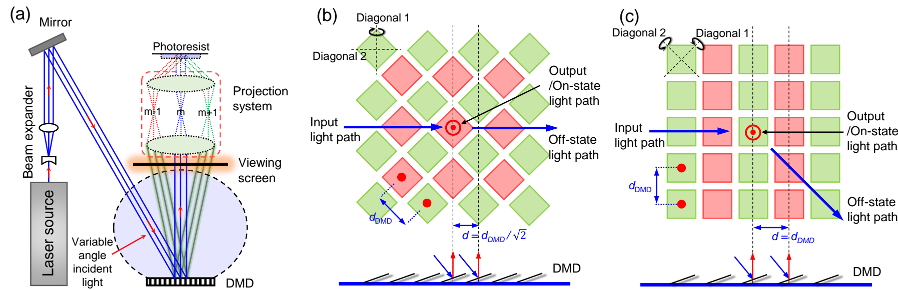

Fig. 1. (a) The schematic diagram of DMD-PL system. (b) The general operation of the DMDs with micromirror pitches of 7.56 μm, 10.8 μm, and 13.68 μm. The micromirror is deflected 12° around the diagonal. The light source is incident on the micromirror along the second diagonal direction, and 24° angle with the normal direction of the substrate. (c) The operation of the DMD with a micromirror pitch of 5.4 μm. The micromirror is first rotated 12° around the diagonal 1 and then rotated 12° around the diagonal 2. The light source is incident on the micromirror along the edge direction at an angle of 34° to the normal direction of the substrate.

As a 2D blazed grating, the spatial distribution of the diffraction angles and orders of the DMD are two-dimensional in nature [39]. We extended the grating diffraction order to the cosine space in which the range of each output order is a dome-shaped space area (Fig. 2(a)). Therefore, the plane distribution of the diffraction orders on the actual observation screen can be mapped to the polar coordinate system in the cosine space. When a bundle of thin parallel light beam is incident on the DMD, the diffracted beams at different angles will be observed on the screen as shown in Fig. 2(a). The incident angle θ_i and azimuth angle φ_i express the trajectory of the light. The angles of the output (diffracted) beam are θ_{mn} and φ_{mn} in the polar coordinate system. In order to visually understand the spatial distribution of diffraction orders, the spatial dot array of diffraction orders can be decomposed into the approximation of one-dimensional blazed gratings in two directions, as shown in Fig. 2(b). The diffraction pattern of the DMD on the entrance pupil plane (or viewing screen in Fig. 1(a)) depending on the DMD's grid morphology is a 2D

Optics EXPRESS

dot array with an equal period (Fig. 2(b)). The above two-dimensional diffraction phenomenon can be described mathematically as follows.

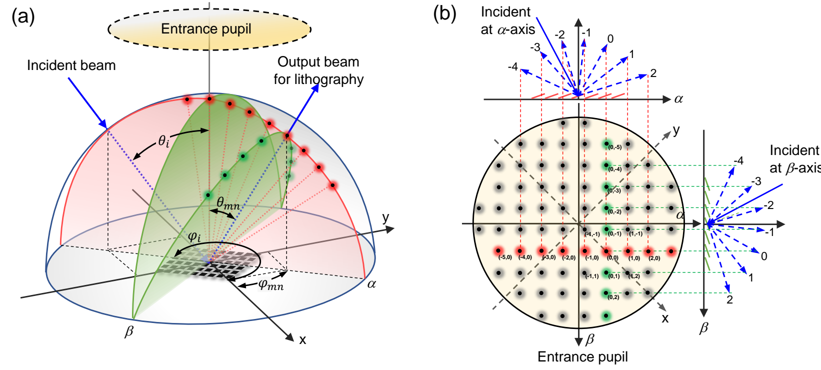

Fig. 2. (a) The schematic diagram of a DMD as a two-dimensional diffraction grating. θ_i is the incident angle and φ_i is the azimuthal angle. The diffraction orders (*m, n*) are distributed on the dome surface. The diffraction angles corresponding to diffraction orders (*m, n*) are θ_{mn} and φ_{mn}. (b) The distribution of diffraction orders (*m, n*) projected onto a plane viewing screen. The 2D diffraction orders (m, n) distribution can be equivalent to a combined mode of diffraction in two orthogonal directions.

The projection distribution of the DMD diffraction orders on the viewing screen at a certain distance can be expressed by the two-dimensional grating equation as follow:

$$\sin\theta_{mn}\cos\varphi_{mn} = \sin\theta_i\cos\varphi_i + m\lambda/d \tag{2}$$

$$\sin\theta_{mn}\sin\varphi_{mn} = \sin\theta_i\sin\varphi_i + n\lambda/d \tag{3}$$

$$x = L\tan\theta_{mn}\cos\varphi_{mn} \tag{4}$$

$$y = L\tan\theta_{mn}\sin\varphi_{mn} \tag{5}$$

where (m, n) denotes the two-dimensional diffraction order, (x, y) is the projection position on the viewing screen, L is the distance between the DMD backplane and the viewing screen, θ_{mn} is the angle of incidence, φ_{mn} is the azimuthal angle, d is the pixel size, and λ is the wavelength of the light source used in the projection lithography. This set of equations can be used to accurately describe the DMD's 2D diffraction orders in a cosine space and their projection positions on the entrance pupil of the optical system.

In DMD, the spatial arrangement of the diffraction orders stems from the constant phase difference of adjacent micromirror elements. A phase model according to the DMD deflection method is established. When DMDs with pixel sizes of 13.68 µm, 10.8 µm, and 7.56 µm are in the "on" state, the micromirror deflects around its main diagonal, and the incident light can be seen as parallel light beams as shown in Fig. 1(b). According to geometric optics, there is a constant phase difference between the adjacent micromirrors in the main diagonal direction, while there is no phase difference in the spatial positions perpendicular to the diagonal direction. By decomposing each plane position on a single micromirror into position parameters about the x-axis and y-axis, the analytical expression of the phase difference Φ caused by the deflection of the micromirror can be obtained by:

$$\Phi = \frac{2\pi}{\lambda}\Delta L = \frac{2\pi}{\lambda}\tan\gamma \cdot (\cos\theta_i + \cos\theta_{mn}) \cdot (y\sin\varphi_i + x\cos\varphi_i) \tag{6}$$

where the deflection angle γ is 12°, θ_i is the incident angle, θ_{mn} is the output diffraction angle, φ_i is the incident azimuthal angle, and x and y are the position parameters of the micromirror in the

xy plane. For the 5.4 µm pixel DMD, the phase difference exists only in the x direction, and the phase difference φ can similarly be expressed by:

$$\Phi = \frac{2\pi}{\lambda}\Delta L = \frac{2\pi}{\lambda}\tan\gamma \cdot (\cos\theta_i + \cos\theta_{mn}) \cdot (x) \tag{7}$$

2.2. DMD diffraction intensity distribution

The complex amplitude distribution of the DMD diffracted light field in entrance pupil can be obtained by the Fourier transform of the light transmittance of the DMD aperture. The entrance pupil of the optical system is positioned in the Fraunhofer diffraction zone, as can be seen by the Fraunhofer diffraction zone judgment: $L \geq D^2/\lambda$, L is the diffraction distance, D is the rectangle side length which is equal to d_{DMD}, λ is the light wavelength. The complex amplitude can be derived as:

$$\tilde{E}(P) = E\sin c(\psi_x)\sin c(\psi_y)e^{-i\delta M/2} \cdot \frac{\sin[(M+1)\delta/2]}{\sin(\delta/2)} \cdot e^{-i\delta N/2} \cdot \frac{\sin[(N+1)\delta/2]}{\sin(\delta/2)} \tag{8}$$

$$\psi_x = d\left(\sin\theta_{mn}\cos\varphi_{mn} - \sin\theta_i\cos\varphi_i - \frac{\xi}{\sqrt{2}}\right) \tag{9}$$

$$\psi_y = d\left(\sin\theta_{mn}\sin\varphi_{mn} + \sin\theta_i\sin\varphi_i - \frac{\xi}{\sqrt{2}}\right) \tag{10}$$

E is the incident light amplitude, ψ_x and ψ_y are the spatial frequencies of a single pixels in the x and y directions, respectively. When the function value of [Sinc] is 1, the corresponding amplitude is the maximum. The remaining part is the phase difference and interference terms between the micromirrors of a single coordinate axis. M and N are the number of micromirrors in the x and y directions, and δ is the phase difference between the micromirrors. When the phase difference δ is equal to the integer multiple of 2π, the coherent light reflected by multiple micromirrors produces constructive superposition. Therefore, the intensity distribution of the diffraction pattern with periodic arrangement is equal to the product of the diffraction factor of single micromirror and the interference factor of the DMD. ξ=(1/λ)·tanγ·(cosθ_i+θ_{mn}) is the spatial frequency shift caused by the deflection of the micromirror. When the pixel is deflected, the incident angle and the diffraction angle change, which will produce a phase difference, and lead to the spatial frequency shift. It can be deduced by Eq. (9) or Eq. (10). The DMD with a 5.4 µm pixel size only has a frequency shift on one single axis, and other DMD have frequency shifts in both x and y axes.

From the above, the diffraction intensity distribution can be derived as:

$$I(P) = I_0\sin c^2(\psi_x)\sin c^2(\psi_y) \cdot \frac{\sin^2[(M+1)\delta/2]}{\sin^2(\delta/2)} \cdot \frac{\sin^2[(N+1)\delta/2]}{\sin^2(\delta/2)} \tag{11}$$

When I_0 is normalized and the interference term is ignored, the relative intensity distribution of the diffraction orders can be used to express the diffraction efficiency of the DMD. The relative diffraction efficiency ($E_{\text{diffraction}} = I / I_0$) of the DMD with a pixel size of 13.68 µm, 10.8 µm, and 7.6 µm can be expressed as:

$$\begin{aligned} E_{\text{diffraction}} &= \sin c^2[d(\sin\theta_{mn}\cos\phi_{mn} - \sin\theta_i\cos\phi_i - \frac{\xi}{\sqrt{2}})] \\ &\cdot \sin c^2[d(\sin\theta_{mn}\sin\phi_{mn} + \sin\theta_i\sin\phi_i - \frac{\xi}{\sqrt{2}})] \end{aligned} \tag{12}$$

The relative diffraction efficiency ($E_{\text{diffraction}} = I \,/\, I_0$) of DMDs with 5.4 μm pixel size is expressed as:

$$\begin{aligned} E_{\text{diffraction}} &= \sin c^2[d(\sin\theta_{mn}\cos\phi_{mn} - \sin\theta_i\cos\phi_i - \xi)] \\ &\cdot \sin c^2[d(\sin\theta_{mn}\sin\phi_{mn} + \sin\theta_i\sin\phi_i)] \end{aligned} \tag{13}$$

Equation (12) and Eq. (13) represent the diffraction efficiencies of a single diffraction order of commercial DMDs, and can be used to analyze the energy utilization rate.

3. Diffraction efficiency of DMD in lithography system

The optical system for projection lithography usually includes an objective lens and a tube lens. As shown in Figure1(a), the diffraction orders of the DMD enter the optical system to expose the photoresist, and each order enters the tube lens has spatial information that can work independently. On the one hand, when the lithographic image plane is at the focal plane, multiple levels will be superimposed on the focal plane to increase the focus energy. On the other hand, when the lithographic image surface is on the defocused surface, imaging in different plane positions will cause the lithographic pattern to be distorted. Moreover, entering multiple diffraction orders in the above two cases will increase the exposure dose and reduce the lithography resolution [40,41]. In summary, when multiple orders enter the lithography system, the energy errors will be caused and the depth of focus will be reduced. Therefore, the diffraction efficiency analysis should be placed on a single order. In order to facilitate the analysis, the distance from the observation screen to the DMD is set to 200 mm.

3.1. Dependence of the diffraction efficiency on pixel size

Based on the DMD diffraction model derived in Section 2, numerical calculations of the diffraction orders and efficiencies were implemented using Python coding. Figure 3(a) illustrates the relationship between the diffraction order and the energy envelope. The energy envelope was determined by the shape of the mirrors (square for the DMD) which was derived from the intensity distribution of the pixel diffraction. The efficiency of the diffraction order was modulated by the energy envelope. Thus, the diffraction order located in the envelope will receive more energy. When the single order was in the center of the envelope, the order was in the blazed state. Figure 3(b-e) shows the spatial distribution of diffraction orders in the energy envelope. The pixel parameters of the selected micromirror were 13.68 μm, 10.8 μm, 7.56 μm, and 5.4 μm, and the incident wavelength was 400 nm. The diffraction order of the DMD with pixel size of 7.56 μm in the center under 343 nm irradiation showed the highest diffraction efficiency, as show in Fig. 3(c).

Diffraction is a physical phenomenon that bends the light by optical limitation. When the wavelength of light source is fixed, the smaller the DMD's pixel size, the more obvious the diffraction effect. This trend can be seen from Fig. 3(b-e). The diffraction angles of adjacent orders become larger as their size decreases. For a given distance and size of the entrance pupil, the number of diffraction orders entering the lithography system will decrease. For lithography, this phenomenon can help the optical system filter out the stray light without using the 4F system, to reduce the instability caused by the superposition of multiple diffraction orders on the image plane.

3.2. Dependence of the diffraction efficiency on wavelength

In DMD-PL systems, the photoresist and resin materials were more reactive to higher photonic energy (shorter light wavelength) resulting in faster cure rates. The relative diffraction efficiencies of the multiple types of DMD in the wideband light covering the entire visible and ultraviolet wavelengths were calculated and analyzed. Figure 4(a) shows the diffraction efficiency distribution of four types of DMD illuminated with lasers of wavelengths of 200-800 nm. The relative

Optics EXPRESS

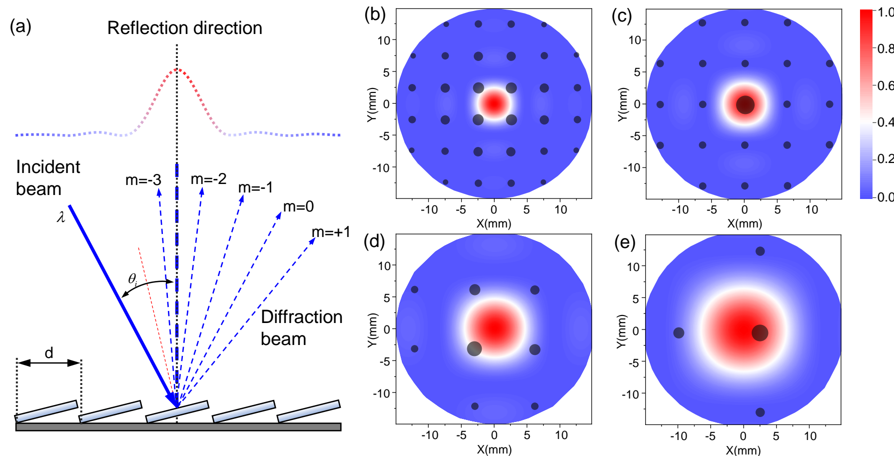

Fig. 3. (a) Schematic diagram of DMD diffraction order and energy envelope. The diffraction orders distribution and light intensity envelope on viewing screen with the various DMD pitches of 13.68 µm (b), 10.8 µm (c), 7.56 µm (d), and 5.4 µm (e). The wavelength of light source is 343nm. The black dots in these figures represent discrete diffraction orders, and their energy envelope is represented by the color bar.

diffraction efficiency oscillated periodically as the wavelength changes from 200 nm to 800 nm. The wavelengths corresponding to the maximum diffraction efficiency were the blaze wavelengths. The numbers of blaze wavelengths when the pixel size changed were different, which were 15, 12, 8, and 12 shown in Fig. 4(a). This regular oscillation of the diffraction efficiencies was caused by the constant change in the matching of the energy envelope and diffraction orders.

In general, only one diffraction order of DMD was needed in the actual lithography as the objection of the lithography system to complete the exposure process. A diffraction order with the highest diffraction energy distribution on the entrance pupil of the objective lens was selected for the following experiments. Taking the DMD with 7.56 µm pixel size as an example, as shown in Fig. 4(b-e), the higher diffraction efficiency is obtained when the diffraction orders [black dots in Fig. 4(b-e)] are closer to the center of the two-dimensional energy envelope. Therefore, the energy utilization of projection lithography can be effectively increased by altering the wavelength.

3.3. Maximizing diffraction efficiency by optimization of condition

As shown in section 3.1, if the working parameters (incident angle θ_i, azimuth angle φ_i) do not achieve the maximum diffraction efficiency for a certain wavelength (“anti-blaze” condition), the lithography energy utilization rate will be greatly reduced. Therefore, it is often possible, in an “anti-blaze” arrangement, to change the incident angle so that one of the orders lines up with the energy envelope peak producing a “blaze” condition. Taking the 343nm and 515 nm as an example, the diffraction efficiencies for the DMD with a 7.56 µm pixel size were 47% and 73%, respectively, when working parameters of 24° incidence angle and 45° azimuthal angle were used. Therefore, when the wavelength of a projection lithography system is determined and unchangeable, it is necessary to optimize the working parameters. An incidence wavelength of 343 nm, a DMD pixel size of 7.56 µm and a fixed azimuth angle of 45° were used for illustration, and the incidence angle was varied to optimize the diffraction efficiency, and the results are shown in Fig. 5(a).

The obtained trend of the diffraction efficiency can be used to optimize the energy utilization of projection lithography. In Fig. 5(a), the diffraction efficiency gradually increased as the incident

Optics EXPRESS

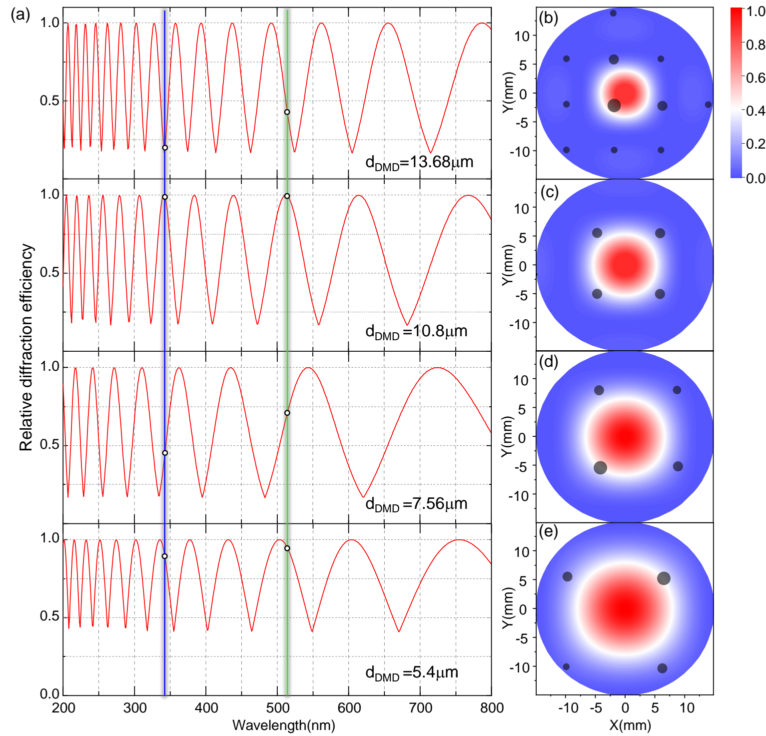

Fig. 4. (a) The diffraction efficiency distribution in the 200 nm - 800 nm band for DMDs with micromirror pixels of 13.68 μm, 10.8 μm, 7.56 μm, and 5.4 μm. The diffraction orders distribution and light intensity envelope on viewing screen with the various incident wavelengths of (b) 300 nm, (c) 400 nm, (d) 500 nm, (e) 600 nm, respectively. The light source is incident on the DMD of 7.56 μm pixel in 24° incidence angle and 45° azimuthal angle.

angle increased and topped at 34°, which is different from the incident angle of 24°. As shown in Figs. 5(b) and 5(d), when the 343 nm light source was incident at 22.5°, the energy envelope was located in the center of the viewing screen, and the diffraction efficiency was not high enough, and this was because the energy was dispersed in multiple orders. In this case, the highest diffraction efficiency was only 40%. When the incident angle was changed to 34° (Fig. 5(c)), a single order with the highest diffraction efficiency appeared as shown in Fig. 5(e). This increase in the efficiency was due to the fact that the diffraction order was located in the center of the energy envelope, and thus the diffraction efficiency could reach 96%. However, in fact, the tilt error, flatness, and structural error of the mirror surface will lead to a decrease in the diffraction efficiency of the ideal calculation. In Fig. 5(e), the energy envelope is in the lower-left corner of the viewing screen. Therefore, in actual projection lithography, the main axis orientation of the optical system needed to be changed so that the highest energy order could be incident on the optical axis. It can be concluded that changing the incident angle can effectively improve the energy utilization of lithography.

Optics EXPRESS

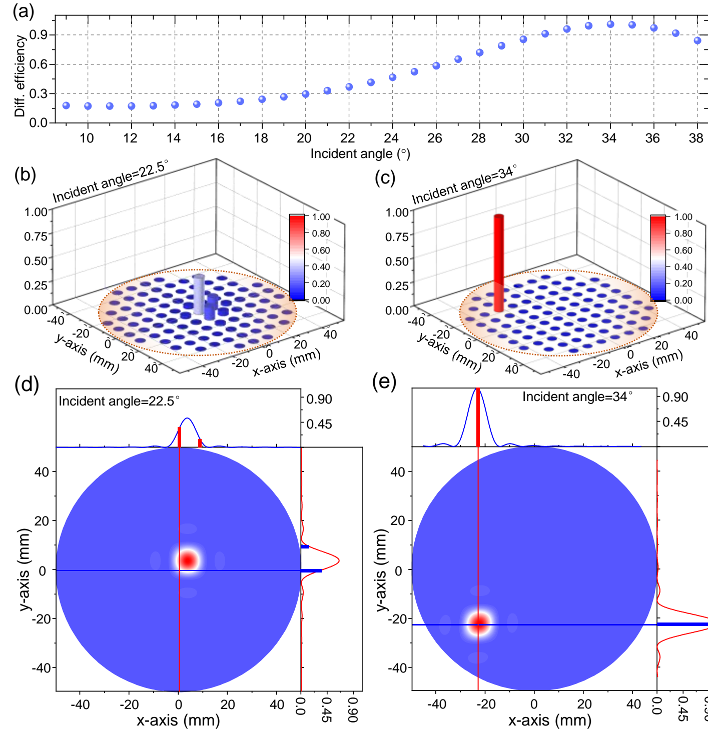

Fig. 5. (a) Diffraction efficiency distribution of a 343nm light source incident on a 7.56µm pixel DMD at a 45° azimuth angle with variable incidence angle. Relative energy distribution of diffraction orders (b) and envelope distribution (d) on a plane viewing screen under 22.5° incident conditions. Relative energy distribution of diffraction orders (c) and envelope distribution (e) on a plane viewing screen under 34° incident conditions

4. Experimental results and analysis

In the experiment, we cannot directly evaluate the absolute diffraction efficiency value $E_{\text{diffraction}}$, because the measured light intensity of diffraction order is affected by the window transmittance, backplane reflectivity, micromirror fill factor. In a coherent imaging lithography systems, we generally focus on the energy utilization of a specific diffraction order in "blaze" condition. The relative value of the diffraction efficiency of different orders can be used to evaluate the optimization effect of energy distribution. Thus, we define an effective energy utilization η_{eff} which is the output power of a single diffraction order over the all diffraction orders power at the entrance pupil plane.

$$\eta_{\text{eff}} = \frac{P_{\text{out},(m,n)}}{\sum\limits_{m,n} P_{\text{out},(m,n)}} = \frac{\eta_{\text{DMD},(m,n)} \cdot P_{\text{int}}}{\sum\limits_{m,n} (\eta_{\text{DMD},(m,n)} \cdot P_{\text{int}})} = \frac{C \times E_{\text{diffraction},(m,n)} \cdot P_{\text{int}}}{\sum\limits_{m,n} (C \times E_{\text{diffraction},(m,n)} \cdot P_{\text{int}})} = \frac{E_{\text{diffraction},(m,n)}}{\sum\limits_{m,n} E_{\text{diffraction},(m,n)}} \tag{14}$$

where $P_{\text{out},(m,n)}$ is the (m,n) order diffracted light intensity, and P_{int} is the total incident light intensity. The angle of two adjacent diffraction orders is $\sin^{-1}(\lambda/d)$. If the angular diameter $\tan^{-1}(a/2L)$ of entrance pupil is smaller than $\sin^{-1}(\lambda/d)$ then it is only possible to capture one order in the output aperture of entrance pupil. In the experiment, the optical power $P_{\text{out},(m,n)}$ was measured using an optical power meter (S120C, Thorlabs), and the optical photograph of diffraction spots on viewing screen is collected via camera (CS235CU, Thorlabs).

Optics EXPRESS

4.1. Energy utilization optimization of single wavelength

In section 3.3, we theoretically analyze that the energy distribution of diffraction order in "anti-blaze" condition can be optimized by changing the incident angle. Figure 6(a) shows the diffraction order and intensity distribution on the observation screen in no optimized incident condition. The flat-top thin light beam at wavelength of 343nm with an incidence angle of 24° and an azimuthal angle of 225° were jointly incidents on a DMD with a pixel size of 7.56 µm. This is a typical diffraction pattern of the "anti-blaze" condition. The four brightest orders contain an amount of energy in the diffraction pattern. The power $P_{\text{out},(m,n)}$ of single diffraction order was measured using an optical power meter and shown in Table 1. Experimental results indicates that these four adjacent orders contain approximately four-fifths of the output energy in entrance pupil, with the remaining one-fifth being distributed in all of the other orders. The effective energy utilization η_{eff} for the diffraction order (6,6) with the greatest energy in the center is about 45%. This lower energy utilization is not suitable for use in lithography systems.

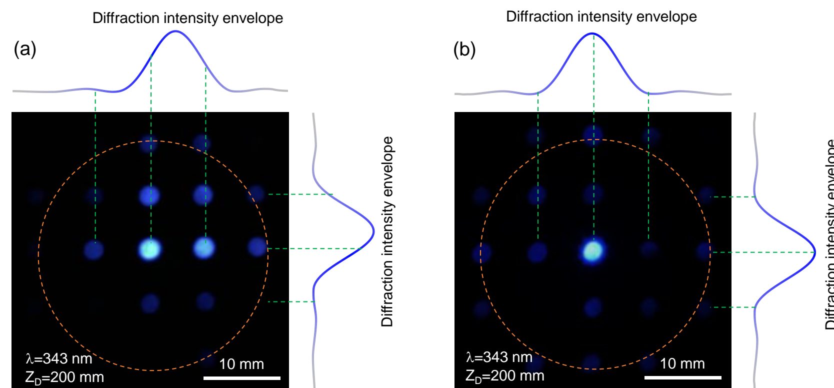

Fig. 6. The diffraction order and intensity distribution on the experimental observation screen. (a) No optimized incident condition that the incident angle is 24° and the azimuth angle is 225°; (a) Optimized incident condition that the incident angle is 34° and the azimuth angle is 225°. The light source wavelength is 343 nm. The distance between the viewing screen and DMD is 200 mm

Table 1. Comparison of theoretical and experimental results of single wavelength illumination.

No optimized angle of incidence (24°)			Optimized angle of incidence (34°)		
Order (m,n); power of single order (µW)			Order (m,n); power of single order (µW)		
(5,5); 2.50	(6,5); 17.00	(7,5); 11.20	(5,5); 3.10	(6,5); 7.30	(7,5); 1.80
(5,6); 6.60	(6,6); 74.12	(7,6); 43.00	(5,6); 6.80	(6,6); 136.00	(7,6); 2.50
(5,7); 1.89	(6,7); 3.70	(7,7); 4.20	(5,7); 1.60	(6,7); 2.50	(7,7); 2.30

Then, we have studied how to transfer the diffraction intensity distribution of the "anti-blaze" condition to the "blaze" condition by changing the angle of incidence. By increasing the incident light angle from 5° to 38° shown in Fig. 5(a), the maximum of energy envelope is gradually moved to a certain diffraction order, rather than allocating four diffraction orders at the same time shown in Fig. 6(b). The positional relationship between the envelope and the diffraction order is visualized on the top and right of the photograph. The measured power $P_{\text{out},(m,n)}$ of single diffraction order is shown in Table 1. Experimental results indicates that the diffraction order

(6,6) in "blaze" condition contains more than 80% of the output energy in entrance pupil, with the remaining fifth being distributed in all of the other orders. The effective energy utilization $\eta_{\rm eff}$ for the diffraction order (6,6) with the greatest energy in the center is about 88%. Obviously, this optimized energy utilization is beneficial for lithography systems.

4.2. Energy utilization optimization of multiple wavelength

Similarly, we also have investigated the simultaneous optimization of lighting conditions to maximize the energy utilization of both wavelengths. We used a projection lithography system with a dual-wavelength illumination to verify the conditions for the optimization of the diffraction efficiency. Two wavelengths of 343 nm and 515 nm femtosecond laser beams through the optical lens pair were collimated into the flat-top light, and two light beams with an incidence angle of 24.5° and an azimuthal angle of 220° were jointly incidents on a DMD with a pixel size of 7.56 μm. The DMD was loaded with a rectangular pattern of 500×500 pixels. To mimic the actual projection objective position, the viewing screen was 200 mm away from the DMD. The diffraction order of the incident light with a wavelength of 343 nm had a symmetric intensity distribution with the diagonal as the central axis (Fig. 7(a)). Its spatial distribution on the viewing screen resembled that of the checkerboard grid, and the on-screen position between each level depended on the angle and azimuth of the laser emission and the distance of the viewing screen from the DMD. Figure 7(b) shows the spatial distribution and energy distribution of the diffraction orders for the incident wavelength of 515 nm. The spacing between the adjacent orders was larger. This was because the 515 nm was longer than 343 nm, and thus the diffraction angle of the adjacent order became larger according to Eq. (1) and Eq. (2). Figure 6(c) shows the diffraction orders of 343 nm and 515 nm entering the DMD with the same incidence angle and azimuthal angle. It can be seen that the highest energy orders of the two wavelengths almost overlapped in the center, and the offset between them was only 0.05 mm. For a projection objective with a certain entrance pupil, two laser beams can enter at the same time without affecting the image quality for lithography.

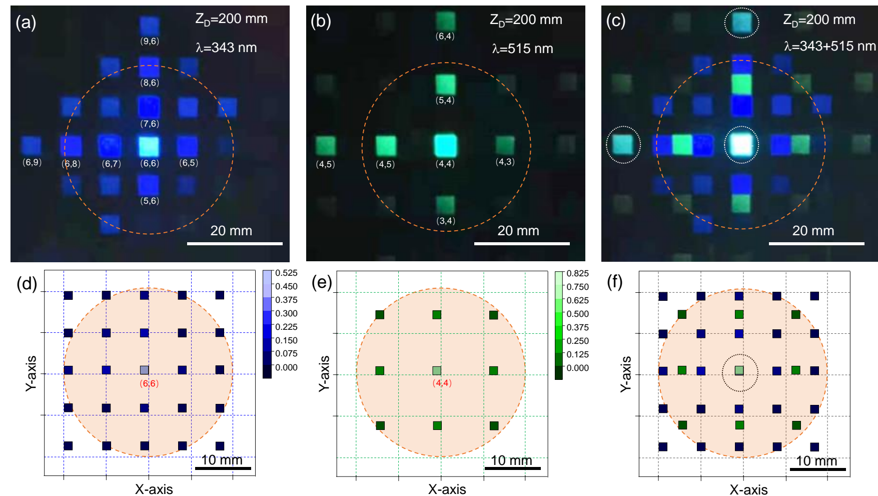

Fig. 7. The diffraction order distribution on the experimental observation screen, the distance between the viewing screen and DMD is 200 mm. The incident angle is 24.5°, the azimuth angle is 220°, and the light source wavelength is 343 nm(a), 515 nm(b), 343 + 515 nm(c). The diffraction order simulation distribution of 343 nm(d), 515 nm(e), 343 + 515 nm (f) incident wavelength.

Optics EXPRESS

Theoretical simulation results using the same incidence conditions were obtained by the python code in Figs. 7(d) and 7(e). The theoretical results showed good agreement with the experimental results. At the same time, the (9,6) and (6,9) levels of 343 nm observed in Fig. 7(c) overlapped with the (6,4) and (4,6) levels of 515, respectively, and this phenomenon was well explained by the theoretical calculations. Figure 7(f) is the simulation result for the situation of Fig. 7(c), exhibiting good agreement between the simulation and the experiment. Table 2 summarizes the measured power of each order together with the calculated diffraction efficiency of the corresponding orders.

Table 2. Comparison of theoretical and experimental results of double-wavelength illumination.

343 nm			515 nm		
Orders	Experimental data $P_{out,(m,n)}$ (μW)	Calculation diffraction efficiency $E_{diffraction,(m,n)}$	Orders	Experimental data $P_{out,(m,n)}$ (μW)	Calculation diffraction efficiency $E_{diffraction,(m,n)}$
(6,6)	14.54	0.481	(4,4)	8.30	0.720
(6,7)	3.17	0.100	(5,4)	0.65	0.056
(7,6)	3.50	0.110	(4,5)	0.70	0.060
(6,5)	0.98	0.027	(4,3)	0.24	0.021
(5,6)	0.99	0.029	(3,4)	0.26	0.022
η_{eff} of "blaze" order	~ 63%	~ 64%	η_{eff} of "blaze" order	~ 82%	~ 82%

It can be seen from Table 2 that there existed an energy maximum at 343 nm and 515 nm, corresponding to (6,6) and (4,4) levels, respectively. We can compare the ratio ($P_{out,(m,n)}$ /P_{max} and $E_{diffraction,(m,n)}/E_{max}$) of in the experimental results and calculated results to verify the correctness of the model. For the 343nm experiment results, the ratios $P_{out,(m,n)}$ /P_{max} of the highest power to other orders in the order of Table 1 were 0.21, 0.24, 0.07 and 0.07 respectively, and the ratios $E_{diffraction,(m,n)}/E_{max}$ of the corresponding model calculation results were 0.21, 0.23, 0.06 and 0.06. For the experiment results of 515 nm wavelength, the ratio of the highest power order to other orders were 0.08, 0.08, 0.03, and 0.03, and the corresponding model calculation results were 0.08, 0.08, 0.03, and 0.03. It can be seen that the ratios were very close, indicating that the model could accurately predict the actual DMD energy distribution of the diffraction orders. At the same time, the energy utilization η_{eff} is close to two-thirds (~ 63% at 343nm) and more than four-fifths (~ 82% at 515nm) under the same optimized incident angle that the incident angle is 24.5° and the azimuth angle is 220°.

5. Conclusion

In this work, we systematically established a 2D grating diffraction model for commercial DMDs, which could accurately predict the diffraction efficiency of diffraction orders used for projection lithography at different operating conditions. The diffraction efficiencies of DMD at the wavelengths of 200 nm-800 nm band simulated by Python coding show that the energy utilization can be improved by properly combining the wavelength and the DMD's pitch size. The maximum diffraction efficiency was optimized by varying the incidence angle for the wavelength of 343 nm and successfully achieved 96%. Experimental validation was performed with the wavelengths of 343 nm and 515 nm, and it was shown that the model could accurately predict the energy distribution as well as the spatial distribution of the actual DMD diffraction orders. The effective energy utilization η_{eff} of single order in "blaze" condition at a 34° angle of incidence

can be optimized up to 88%. This work not only establishes a more comprehensive understanding of the diffraction performances of DMD, but also provides an effective tool for maximizing the light energy utilization in DMD-PL.

Funding. Guangzhou Basic and Applied Basic Research Project (202102020999); Natural Science Foundation of Guangdong Province (2020A1515011529); National Natural Science Foundation of China (62005097, 62174071); Science and Technology Planning Project of Guangzhou (202007010002); National Key Research and Development Program of China (2016YFA0200502).

Disclosures. The authors declare that there are no conflicts of interest related to this article.

Data availability. Data underlying the results presented in this paper are not publicly available at this time but maybe obtained from the authors upon reasonable request.

References

1. H. Martinsson, T. Sandstrom, A. J. Bleeker, and J. D. Hintersteiner, "Current status of optical maskless lithography," J. Micro/Nanolithogr., MEMS, MOEMS **4**(1), 011003 (2005).
2. Z. M. Zhang, Q. W. Meng, and N. N. Luo, "A DMD based UV lithography method with improved dynamical modulation range for the fabrication of curved microstructures," AIP Adv. **11**(4), 045008 (2021).
3. J. B. Kim and K. H. Jeong, "Batch fabrication of functional optical elements on a fiber facet using DMD based maskless lithography," Opt. Express **25**(14), 16854–16859 (2017).
4. A. Waldbaur, B. Waterkotte, K. Schmitz, B. E. Rapp, and Rapp, "Maskless projection lithography for the fast and flexible generation of grayscale protein patterns," Small **8**(10), 1570–1578 (2012).
5. Z. M. Zhang, Y. Q. Gao, N. N. Luo, and K. J. Zhong, "Fast fabrication of curved microlens array using DMD-based lithography," AIP Adv. **6**(1), 015319 (2016).
6. Q. Zheng, J. Zhou, Q. Chen, L. Lei, K. Wen, and Y. Hu, "Rapid prototyping of a dammann grating in DMD-based maskless lithography," IEEE Photonics J. **11**(6), 1–10 (2019).
7. C. Peng, Z. Z. Zhang, J. X. Zou, and W. M. Chi, "A high-speed exposure method for digital micromirror device based scanning maskless lithography system," Optik **185**, 1036–1044 (2019).
8. D. Jin, R. J. Zhou, Z. Yaqoob, and P. T. C. So, "Dynamic spatial filtering using a digital micromirror device for high-speed optical diffraction tomography," Opt. Express **26**(1), 428–437 (2018).
9. Y. Zhang, J. Luo, Z. Xiong, H. Liu, L. Wang, Y. Y. Gu, Z. F. Lu, J. H. Li, and J. P. Huang, "User-defined microstructures array fabricated by DMD based multistep lithography with dose modulation," Opt. Express **27**(22), 31956–31966 (2019).
10. R. H. Chen, H. Liu, H. L. Zhang, W. J. Zhang, J. Xu, W. B. Xu, and J. H. Li, "Edge smoothness enhancement in DMD scanning lithography system based on a wobulation technique," Opt. Express **25**(18), 21958–21968 (2017).
11. Q. M. Chen, J. Y. Zhou, Q. Zheng, and Y. M. Hu, "Multi-layer lithography using focal plane changing for SU-8 microstructures," Mater. Res. Express **7**(6), 065306 (2020).
12. Y. H. Liu, Y. Y. Zhao, X. Z. Dong, M. L. Zheng, F. Jin, J. Liu, X. M. Duan, and Z. S. Zhao, "(/12 super resolution achieved in maskless optical projection nanolithography for efficient cross-scale patterning," Nano Lett. **21**(9), 3915–3921 (2021).
13. Y. H. Liu, Y. Y. Zhao, X. Z. Dong, M. L. Zheng, F. Jin, J. Liu, X. M. Duan, and Z. S. Zhao, "Multi-scale structure patterning by digital-mask projective lithography with an alterable projective scaling system," AIP Adv. **8**(6), 065317 (2018).
14. Z. Xiong, H. Liu, R. H. Chen, J. Xu, Q. K. Li, J. H. Li, and W. J. Zhang, "Illumination uniformity improvement in digital micromirror device based scanning photolithography system," Opt. Express **26**(14), 18597–18607 (2018).
15. K. Wen, Y. Ma, M. Liu, J. L. Li, Z. Zalevsky, and J. J. Zheng, "Transmission Structured Illumination Microscopy for Quantitative Phase and Scattering Imaging," Front. Phys. **8**(667), 630350 (2021).
16. B. Smith, B. Hellman, A. Gin, A. Espinoza, and Y. Takashima, "Single chip lidar with discrete beam steering by digital micromirror device **"** Opt," Opt. Express **25**(13), 14732–14745 (2017).
17. Q. Han, J. Z. Zhang, J. Wang, and Q. Sun, "Diffraction analysis for DMD-based scene projectors in the long-wave infrared," Appl. Opt. **55**(28), 8016–8021 (2016).
18. Texas Instrument, Inc., "DMD Optical Efficiency for Visible Wavelengths" (rev. 2019). https://www.ti.com/lit/pdf/dlpa083.
19. Texas Instrument, Inc., "DMD Optical Efficiency for Visible Wavelengths System Design Considerations Using TI DLP® Technology down to 400 nm" (rev. 2014). https://www.ti.com/lit/pdf/dlpa052.
20. Texas Instrument, Inc., "System Design Considerations Using TI DLP® Technology in UVA" (rev. 2020). https://www.ti.com/lit/pdf/dlpa060.
21. B. Hellman, C. Luo, G. Chen, J. Rodriguez, C. Perkins, J.-H. Park, and Y. Takashima, "Single-chip holographic beam steering for lidar by a digital micromirror device with angular and spatial hybrid multiplexing," Opt. Express **28**(15), 21993–22011 (2020).
22. B. Hellman and Y. Takashima, "Angular and spatial light modulation by single digital micromirror device for multi-image output and nearly-doubled étendue," Opt. Express **27**(15), 21477–21496 (2019).

Optics EXPRESS

23. P. F. Van Kessel, L. J. Hornbeck, R. E. Meier, and M. R. Douglass, "A MEMS-based projection display," Proc. IEEE **86**(8), 1687–1704 (1998).
24. K. Kim, S. Han, J. Yoon, S. Kwon, H. K. Park, and W. Park, "Lithographic resolution enhancement of a maskless lithography system based on a wobulation technique for flow lithography," Appl. Phys. Lett. **109**(23), 234101 (2016).
25. Y. L. Meng, W. Lin, C. L. Li, and S. C. Chen, "Fast two-snapshot structured illumination for temporal focusing microscopy with enhanced axial resolution," Opt. Express **25**(19), 23109–23121 (2017).
26. R. S. Ketchum and P. A. Blanche, "Diffraction efficiency characteristics for MEMS-based phase-only spatial light modulator with nonlinear phase distribution," Photonics **8**(3), 62 (2021).
27. X. Chen, B. B. Yan, F. J. Song, Y. Q. Wang, F. Xiao, and K. Alameh, "Diffraction of digital micromirror device gratings and its effect on properties of tunable fiber lasers," Appl. Opt. **51**(30), 7214–7220 (2012).
28. M. Q. Li, Y. N. Li, W. H. Liu, L. Amit, S. Jiang, D. Y. Jin, H. P. Yang, S. Wang, K. Zhanghao, and P. Xi, "Structured illumination microscopy using digital micro-mirror device and coherent light source," Appl. Phys. Lett. **116**(23), 233702 (2020).
29. K. H. Dou, X. P. Xie, M. B. Pu, X. L. Ma, C. T. Wang, and X. G. Luo, "Off-axis multi-wavelength dispersion controlling metalens for multi-color imaging," Opto-Electron. Adv. **3**(4), 19000501 (2020).
30. Q. Geng, D. Wang, P. F. Chen, and S. C. Chen, "Ultrafast multi-focus 3-D nano-fabrication based on two-photon polymerization," Nat. Commun. **10**(1), 2179 (2019).
31. S. K. Saha, D. Wang, H. Nguyen, Y. N. Chang, J. S. Oakdale, and S. C. Chen, "Scalable submicrometer additive manufacturing," Science **11**(6), 1–10 (2019).
32. D. Loterie, P. Delrot, and C. Moser, "High-resolution tomographic volumetric additive manufacturing," Nat. Commun. **11**(1), 852 (2020).
33. Z. Xiong, H. Liu, X. Q. Tan, Z. W. Lu, C. X. Li, L. W. Song, and Z. Wang, "Diffraction analysis of digital micromirror device in maskless photolithography system," J. Micro/Nanolithogr., MEMS, MOEMS **13**(4), 043016 (2014).
34. H. Ryoo, D. W. Kang, and J. W. Hahn, "Analysis of the effective reflectance of digital micromirror devices and process parameters for maskless photolithography," Microelectron. Eng. **88**(3), 235–239 (2011).
35. L. W. Liang, J. Y. Zhou, L. L. Xiang, B. Wang, K. H. Wen, and L. Lei, "Simulation of the effect of incline incident angle in DMD maskless lithography," J. Phys.: Conf. Ser. **844**, 012031 (2017).
36. J. P. Liu, H. Horimai, X. Lin, J. Y. Liu, Y. Huang, and X. D. Tan, "Optimal micro-mirror tilt angle and sync mark design for digital micro-mirror device based collinear holographic data storage system," Appl. Opt. **56**(16), 4779–4784 (2017).
37. M. N. Sing, T. A. Bartlett, W. C. McDonald, and J. M. Kempf, "Super resolution projection: leveraging the MEMS speed to double or quadruple the resolution," Proc. SPIE **10932**, 109320R (2019).
38. J. D. Jackson, "Visual Analysis of a Texas Instruments Digital Micromirror Device," (The Institute of Optics University of Rochester). http://www2.optics.rochester.edu/workgroups/cml/opt307/spr05/john/
39. J. E. Harvey and C. L. Vernold, "Description of diffraction grating behavior in direction cosine space," Appl. Opt. **37**(34), 8158–8159 (1998).
40. J. H. Liu, J. B. Liu, Q. Y. Deng, J. H. Feng, S. L. Zhou, and S. Hu, "Intensity modulation based optical proximity optimization for the maskless lithography," Opt. Express **28**(1), 548–557 (2020).
41. S. P. Guo, Z. F. Lu, Z. Xiong, L. Huang, H. Liu, and J. H. Li, "Lithographic pattern quality enhancement of DMD lithography with spatiotemporal modulated technology," Opt. Lett. **46**(6), 1377–1380 (2021).